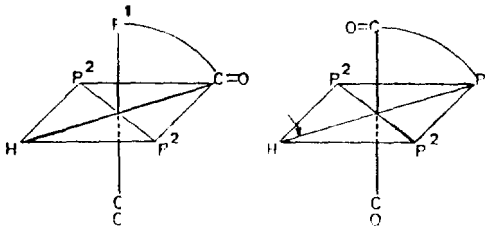

E F

tween hydride and cis phosophorus (3-20HZ). The small coupling constants of **1** indicate that the hydride is cis to the phosphorus. Therefore, the possible structure of **F** will be eliminated.

The $^{31}P\{H\}$ NMR spectrum (See Figure 2) provides additional information on the structure of **3**. It consists of one doublet and one triplet due to the spin coupling between the chemically equivalent two phosphine ligands and one phosphine ligand, corresponding to the AX_2 spin system. This pattern is very similar to that of the compound $Os(PMe_2Ph)_3Cl_2(MeCN)$[17], which has the mirror plane formed by one phosphine, MeCN and two chlorine. Accordingly, from our experimental observations, the correct structure of the compound **3** appears to favor the structure **E**. The complexes of **1**, **2**, and **4** can be similarly assigned as the complex **3**.

In further studies, we are investigating the possibility of carbon-carbon bond cleavage under the same condition.

Acknowledgements. We wish to thank the Korea Science and Engineering Foundation for the financial support.

References

1. G.W. Parshall, *J. Mol. Catal.*, **4**, 243 (1978) 243.
2. *Chem. Eng. New.*, **54**, 25 (1976).
3. Jae J. Koh, W.H. Lee, P.G. Williard and W.M. Risen, *J. Organomet. Chem.*, **284**, 409 (1985).
4. J.W. Suggs, *J. Am. Chem. Soc.*, **100**, 640 (1978).
5. J.W. Suggs. *J. Am. Chem. Soc.*, **101**, 489 (1979).
6. D. Milstein, *Acc. Chem. Res.*, **17**, 221 (1984).
7. T.B. Rauchfuss, *J. Am. Chem. Soc.*, **101**, 1045 (1979).
8. E.F. Landvatter and T.B. Rauchfuss, *Organometallics*, **1**, 506 (1982).
9. J.W. Suggs and C.H. Jun, *J. Am. Chem. Soc.*, **106**, 3054 (1984).
10. C.A. Reed and W.R. Roper, *J. Chem. Soc., Dalton Trans.* 1365, 1973.
11. J.P Collman, N.W. Hoffman, and J.W. Hosking, *Inorganic Syntheses* **XII**, 8.
12. G.P. Schiemenz and H. Kaack, *Liebigs Ann. Chem.*, 1940, (1973).
13. A. Kirpnal and E. Reiter, *Chem. Ber.*, **60**, 664 (1927).
14. M. Ciriano, M. Green, J.A.K. Howard, J. Proud, J.L. Spencer, F.G.A. Stone, and C.A. Tsipis, *J. Chem. Soc. Dalton Trans*, 801 (1978).
15. R.H. Crabtree and R.J. Uriate, *Inorg. Chem.* **22**, 4152 (1983).
16. R.H. Crabtree, J.W. Faller, M.F. Mellea and J.M. Quirk, *Organometallics*, **1**, 1361, 1982.
17. V.T. Coombe, G.A. Heath, T.A. Stephenson, J.D. Whitelock, and L.J. Yellowlees, *J. Chem. Soc. Dalton Trans*, 947 (1985).

Transport Mechanisms and Defect Structures of the System α-Fe_2O_3-CoO

Keu Hong Kim*, Sung Han Lee, and Jae Shi Choi

Department of Chemistry, Yonsei University, Seoul 120. *Received May 15, 1986*

The electrical conductivity of the system α-Fe_2O_3-CoO was measured in the temperature range 200-1000°C and P_{O_2} range 10^{-7}-2×10^{-1} atm. Possible defect models were suggested on the basis of conductivity data, which were measured as a function of temperature and of oxygen partial pressure. The observed activation energies were 0.50 eV and 1.01 eV in the low- and high-temperature regions, respectively. The observed conductivity dependences on P_{O_2} were $\sigma \propto P_{O_2}^{-1/6}$ in the P_{O_2} range 10^{-7}-10^{-4} atm and $\sigma \propto P_{O_2}^{-1/4}$ at P_{O_2}'s of 10^{-4}-2×10^{-1} atm at temperatures from 300-1000°C. An extrinsic electron conduction due to an $V_O^{\cdot\cdot}$ defect and an intrinsic electron conduction due to an $Fe_i^{\cdot}$ defect were suggested at different temperature and oxygen partial pressure regions, respectively.

Introduction

Fe_2O_3 is known to be metal excess,[1,2] oxygen deficient[3], and an intrinsic semiconductor,[4,5] while FeO and Fe_3O_4 are metal deficient p-type semiconductors, represented as $Fe_{1-x}O$[6-8] and $Fe_{3-x}O_4$[1,9], respectively. Salmon[1] suggested that predominant defects in Fe_2O_3 are oxygen vacancies or interstitial iron ions.

Two surface sites, probably an Fe^{2+} interstitial and an oxygen vacancy were suggested by Kim *et al*[10] from the kinetic measurements of the oxidation of CO on α-Fe_2O_3 which was prepared by $FeCl_2$ and KOH according to the Balz method.[11] The oxygen vacancy was also found from the measurements of conductivities on α-Fe_2O_3[12], Ni-doped α-Fe_2O_3[13], and Cd-doped α-Fe_2O_3[14,15] at temperatures from 250 to 460°C under various Pco, P_{SO_2}, and P_{O_2} conditions. The conductivity data showed that the adsorption of O_2 on pure and doped α-Fe_2O_3 withdraws the conduction electrons from an

oxygen vacancy, while CO and SO_2 donates electrons to the conduction band.[12-14]

The electrical conduction mechanism in α-Fe_2O_3 has been generally proposed as a wide band conduction or a hopping conduction of small polaron in a narrow band. The microwave and dc conductivity of α-Fe_2O_3 have been measured at temperatures from 925 to 1194°C in air, and a polaron below 925°C and free carriers above 925°C were suggested as the electrical conduction mechanisms of α-Fe_2O_3.[16] Mochizuki interpreted α-Fe_2O_3 as an intrinsic semiconductor in the temperature range from 925 to 1194°C. Gardner *et al.*,[3] on the other hand, reported that α-Fe_2O_3 was an extrinsic semiconductor at temperatures below 800°C.

In this investigation, dc conductivities of the systems α-Fe_2O_3: 0.53 mol % CoO, α-Fe_2O_3: 1.02 mol % CoO, and α-Fe_2O_3: 1.51 mol % CoO were measured as a function of temperature and an oxygen partial pressure in the temperature range 200 to 1000°C and Po_2 range 10^{-7} to 2×10^{-1} atm.

Experimental

Sample preparations: Pure α-Fe_2O_3:[17,18] $Fe(NO_3)_3\cdot9H_2O$ solution in water was added to 6% aqueous ammonia with constant stirring. The precipitate was washed with distilled water until the washed liquor was free from nitrates and then dried at 50°C. The product was heated at 200°C for 10 hrs with a dry stream of air in order to remove the water. The phase of α-Fe_2O_3 was identified by x-ray powder technique. The x-ray pattern showed a fine α-Fe_2O_3 phase. The atomic absorption spectroscopy (A.A.S.) showed that α-Fe_2O_3 powder contains less than 153 ppm of total impurities such as Ni, Cu, Mn, Ca, Mg, etc.

The systems α-Fe_2O_3-CoO: Fine powders of α-Fe_2O_3 and CoO (obtained from Johnson Matthey Co. 99.99%) were uniformly dispersed in various mol ratios with chemically pure ethanol for 72 hrs and then dried at 200°C. α-Fe_2O_3-CoO solid solutions were prepared by the direct solid-state reaction between the relatively high m.p. CoO and low m.p. α-Fe_2O_3. The fine powders of α-Fe_2O_3 and CoO were sintered at 800°C for 10 hrs and annealed at 1350°C for 72 hrs in covered platinum crucible and cooled slowly to room temperature in order to minimize the defects produced by heating. The preheated specimen was etched in dilute HNO_3 and $(NH_4)_2S_2O_8$. The amount of CoO incorporated into α-Fe_2O_3 was determined by A.A.S. and found to be 0.53, 1.02, and 1.51 mol %, respectively. The α-Fe_2O_3 samples doped with 0.53, 1.02, and 1.51 mol % CoO were compressed into pellets under 196 MPa in vacuum and then heated at 1350°C for 10 hrs. The pellet density measured by the mercury immersion method showed 96% of the theoretical density, with an average grain size of approximately 6.13 μm. The specimen had 4-5% porosity and the average pore size was approximately 0.72 μm. The pellet was cut into a rectangular form, $1.2\times0.65\times0.20$ cm³ in size, by diamond cutter and polished flat using α-Fe_2O_3 powder as an abrasive. Before the sample was introduced into the sample basket, it was always etched in $(NH_4)_2S_2O_8$ and dilute HNO_3, and washed with distilled water, dried, and then connected to the Pt probes.

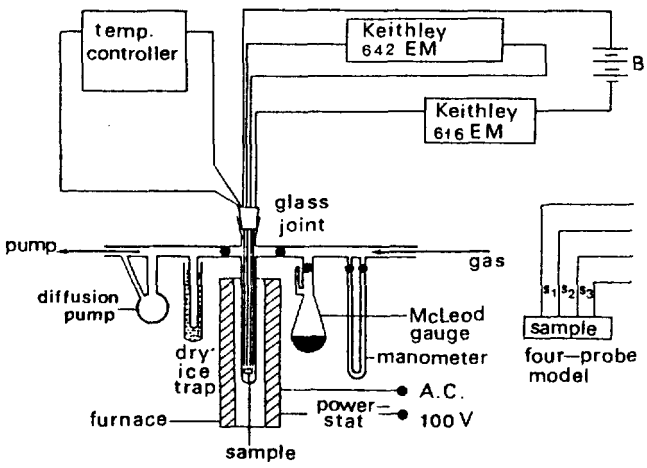

Figure 1. Schematic drawing of the conductivity measurement circuitry and the four-probe model.

Po_2 establishment. The various oxygen partial pressures were established using pure oxygen or nitrogen, and or a mixture of 0.001% oxygen in nitrogen obtained from Matheson Gas Products. The quartz sample basket was evacuated to a pressure of 1×10^{-7} torr by the diffusion pump[19] at room temperature, and then the temperature of the sample container was increased up to 200°C. A mixture of oxygen and nitrogen, or pure oxygen, was introduced into the sample basket, which was then evacuated again to a pressure of 1×10^{-6} torr. The introduction and evacuation of gas at 200°C were performed two or three times, and then total pressure was controlled with 0.001% oxygen in nitrogen in order to establish the required Po_2. The pressures of the evacuated sample container and the O_2-N_2 mixture were read on a McLeod gauge, a thermocouple gauge, Pirani gauge, and an ultra-high vacuum ionization gauge, respectively.

Conductivity measurement. Measurements of electrical conductivity were performed according to the Valdes' technique,[20] which was briefly described in the previous articles.[21,22] This technique has also been employed to measure the electrical conductivity of other oxide semiconductors; for example, α-Fe_2O_3/α-Fe_2O_3: Cd,[10,12,14,15] La_2O_3: Cd,[23] Sm_2O_3,[24] H_2-Reduced Rutile,[25] $SrTiO_3$: Ni/CO-Reduced $SrTiO_3$: Ni,[26] and Tm_2O_3.[27] A schematic diagram of the conductivity cell, the cell geometry, electrical circuit, and four-probe was shown in Figure 1. Details have been described for the vacuum system,[28] instruments,[29] and the conductivity calculation procedure.[21,22] The current through the sample was maintained from 10^{-7} to 10^{-2} A by a rheostat and the potential across the inner two probes were maintained between 0.3 and 1.7 V. The potential difference was measured by a Keithley 642 digital multimeter, and the current through the sample was measured by a Keithley 616 digital electrometer. The measurements of electrical conductivity were performed over a cycle in the temperature range 200-1000°C under Po_2's from 10^{-7}-2×10^{-1} atm, starting from the low temperature end, proceeding toward the high temperature end, and then back again to the lower end. The sample was held at each temperature until equilibrium between the oxygen phase and sample was achieved, indicated by a constant conductivity.

Results and Discussion

Temperature dependence of electrical conductivity. Electrical conductivities were investigated as a function of temperature and an oxygen partial pressure(Po_2). Figure 2

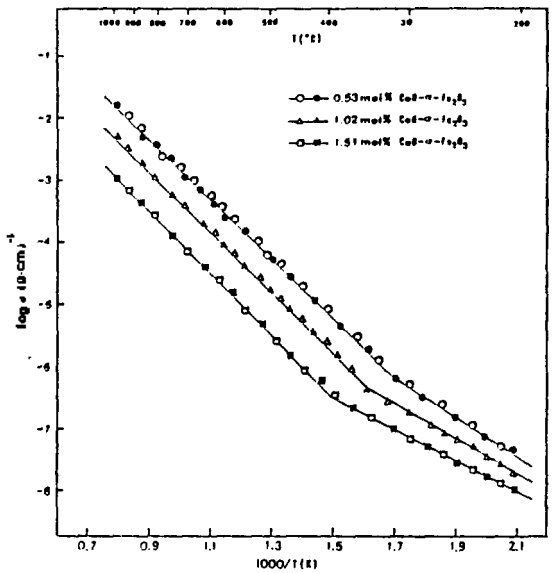

Figure 2. Electrical conductivities of α-Fe_2O_3: CoO as a function of reciprocal absolute temperature at constant oxygen partial pressure of 2×10^{-1} atm.-O-△-□-: data measured at increasing temperature; -●-▲-■-: data measured at decreasing temperature.

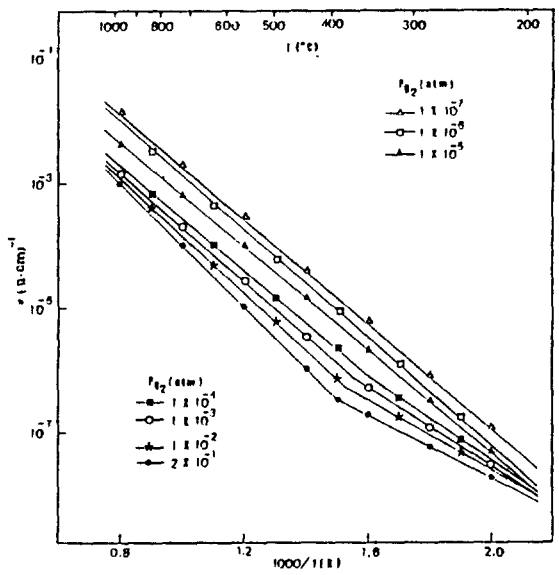

Figure 3. Temperature dependence of electrical conductivity of α-Fe_2O_3: 1.51 mol % CoO at constant oxygen partial pressures.

shows the log σ *vs.* 1/T for 0.53, 1.02, and 1.51 mol % CoO-doped α-Fe_2O_3 at temperatures from 200 to 1000°C and Po_2 of 2×10^{-1} atm. The electrical conductivity data measured at increasing temperature are in good agreement with the data measured at decreasing temperature for all CoO-doped α-Fe_2O_3 samples. From the electrical conductivity dependences on temperature in Figure 2, two regions are possibly assumed: The low- and high- temperature portions of the log σ *vs.* 1/T plots are the extrinsic and intrinsic regions, respectively. At Po_2 of 2×10^{-1} atm all samples show the distinct extrinsic

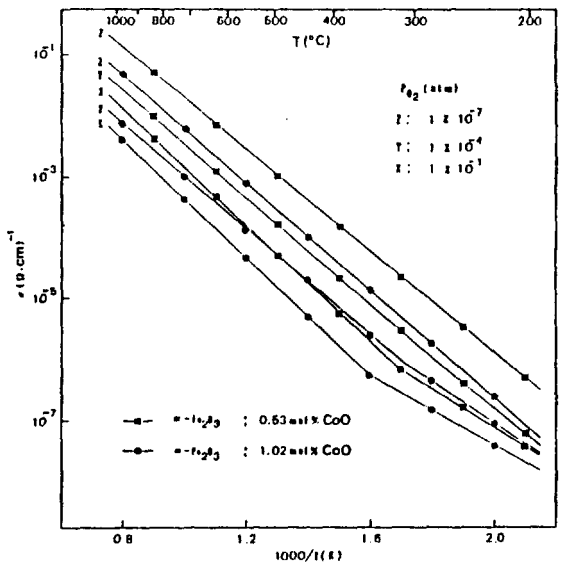

Figure 4. Conductivity isobars of α-Fe_2O_3: 1.02 and α-Fe_2O_3: 0.53 mol % CoO at three typical oxygen partial pressures.

Table 1. Observed Activation Energies(eV) for the Conductivity of Pure and Doped α-Fe_2O_3

Gardner *et al.*[3]	Tannhauser[30]	Geiger & Wagner[31]	Chang & Wagner[31]	This work	
				high temp.	low temp.
1.00	1.07	1.15	1.18	1.01	0.50

regions and inflection points appear in the temperature range 300–400°C, indicating all the experimental curves of log σ *vs.* 1/T plots to be linear at the low- and high-temperature regions away from the inflection points.

Activation energy obtained by the least-square method from the conductivity-temperature data for 1.51 mol % CoO-doped α-Fe_2O_3 is 0.50 eV for the extrinsic region and 1.01 eV for the intrinsic region. Table 1 shows the activation energies for the conductivity of pure and doped α-Fe_2O_3 observed by several workers.[3, 30-32] As shown in Table 1, the activation energy(1.01 eV) for the high temperature region is in good agreement with the values of Gardner *et al.*[3] and Tannhauser[30] and is in reasonable accordance with those of Geiger and Wagner[31] and Chang and Wagner.[32] From good or reasonable agreement of an activation energy in the high temperature region, the intrinsic conductivity of the CoO-doped α-Fe_2O_3 is confirmed at Po_2 of 2×10^{-1} atm.

Figure 3 shows the temperature dependence of electrical conductivity for 1.51 mol % CoO doped α-Fe_2O_3 at Po_2's of 10^{-7} to 2×10^{-1} atm. As shown in this figure, the extrinsic conductivities disappear at Po_2's lower than 1×10^{-4} atm. As can be seen in Figure 4, the extrinsic conductivity vanishes even at Po_2 of 1×10^{-4} atm for 0.53 mol % CoO-doped α-Fe_2O_3. This extension of the extrinsic region to the lower Po_2 with increasing doping level indicates that some parts of the intrinsic region in n-type α-Fe_2O_3 change to the extrinsic region due to impurity doping. This change of the intrinsic to the extrinsic appears at the temperature lower than 300–400°C,

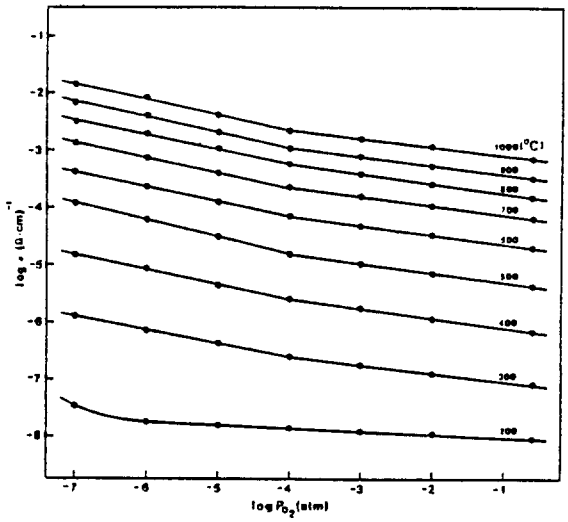

Figure 5. Conductivity isotherms of α-Fe_2O_3: 1.51 mol % CoO as a function of oxygen partial pressure.

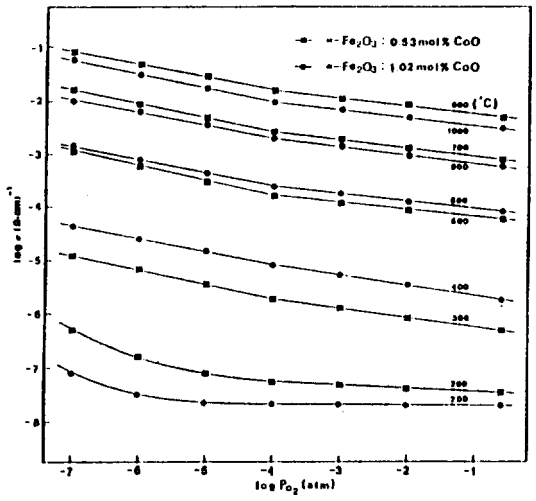

Figure 6. Conductivity isotherms of α-Fe_2O_3: 1.02 and α-Fe_2O_3: 0.53 mol % CoO as a function of oxygen partial pressure.

regardless of the doping level.

Po_2 dependence of Electrical Conductivity. Figure 5 shows the conductivity isotherms of 1.51 mol % CoO-doped α-Fe_2O_3 as a function of Po_2. The conductivity increases with decreasing Po_2 at constant temperature. A similar increase in conductivity with decreasing Po_2 is seen in 1.02 and 0.53 mol % CoO-doped α-Fe_2O_3, as shown in Figure 6. In Figures 5 and 6, the conductivity dependences on Po_2 are approximately fixed, regardless of the dopant level of CoO in α-Fe_2O_3. However, at 200°C it is difficult to evaluate the slope in log σ *vs.* log Po_2 plot for three samples. In the temperature range 300 - 1000°C, log σ *vs.* log Po_2 shows a discontinuity at Po_2 of 1×10^{-4} atm for all samples, as shown in Figures 5 and 6. This indicates that the conduction mechanism is the same for the three different samples. The $-1/n$ values in $\sigma \propto Po_2^{-1/n}$ are listed in Table 2 at the various temperatures investigated. As shown in Table 2, $-1/n$ values are approximately 1/4 and 1/6 at low ($<10^{-4}$ atm) and high ($>10^{-4}$ atm) pressure regions, respectively. Because two different defect structures may

Table 2. Electrical Conductivity Dependence on PO for α-Fe_2O_3 Doped with Various CoO Contents (mol %) at Measured Temperatures

Temperature(°C)	$-1/n$ (average values)	
	Low Pressure Region ($<10^{-4}$ atm)	High Pressure Region ($\geq10^{-4}$ atm)
200	—	—
300	1/4.3	1/6.5
400	1/4.0	1/5.8
500	1/4.3	1/6.0
600	1/4.1	1/6.0
700	1/4.2	1/6.0
800	1/3.9	1/6.0
900	1/3.8	1/6.3
1000	1/4.0	1/6.5

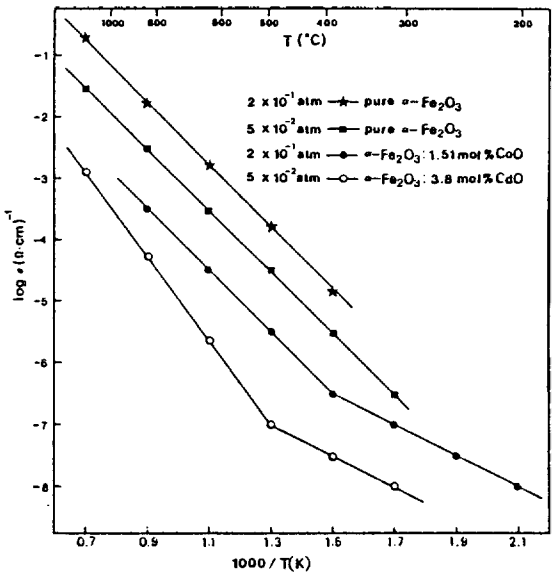

Figure 7. Comparative electrical conductivities of pure α-Fe_2O_3, α-Fe_2O_3: CdO, and α-Fe_2O_3: CoO at constant oxygen partial pressures. -★-: data from ref.(3); -O-■-: data from ref.(15); -●-: present work.

originate from 1/4 and 1/6, the error in the slope measurement is critical. It is generally believed that this log σ *vs.* log Po_2 plot is insensitive to a small change of slope. However, our test plots of σ *vs.* $Po_2^{-1/n}$ at several measured temperatures give the same slope as those in the log σ *vs.* log Po_2 plots, showing a straight lines away from Po_2 of 1×10^{-4} atm.

Figure 7 shows the comparative electrical conductivities of pure α-Fe_2O_3, α-Fe_2O_3: CdO, and α-Fe_2O_3: CoO at constant Po_2's. As shown in this figure, the slope of the intrinsic region in Arrhenius plot for α-Fe_2O_3: 1.51 mol % CoO is in good agreement with the slopes of pure α-Fe_2O_3 at Po_2's of 2×10^{-1} atm[3] and 5×10^{-2} atm,[15] however it is somewhat different from the slope of α-Fe_2O_3: 3.8 mol % CdO. The activation energy for 3.8 mol % CdO-doped α-Fe_2O_3 is 1.34 eV and inflection point appears at about 500°C. These large activation energy and high-temperature inflection point in comparison with 1.01 eV and 400°C for 1.51 mol % CoO-doped

α-Fe_2O_3 indicate that the conduction mechanism may be different in the intrinsic region, and the extrinsic region extends to the high temperature side. However, the activation energy (0.51 eV) in the extrinsic region is exactly same for CdO- and CoO-doped α-Fe_2O_3 samples. This indicates that the conduction mechanism in extrinsic region may be unique for two samples.

Electrical Conduction Mechanisms

Intrinsic region (Po_2<10^{-4} atm). The activation energy and Po_2 dependence of electrical conductivity are 1.01 eV and $\sigma \propto Po_2^{-1/4}$, respectively. At Po_2 lower than 10^{-4} atm, the electrical conductivity of α-Fe_2O_3: CoO shows the typical intrinsic conductivity. α-Fe_2O_3: CoO was already annealed at 1350°C, and in addition to heating, α-Fe_2O_3 was readily doped with impurity. By heating α-Fe_2O_3 at high temperature, oxygen vacancy can be produced.[1, 33-35] The diffusion of lattice oxygen may supply electrons for the conduction band by the following disorder

$$O_o \rightleftharpoons V_o^{\cdot\cdot} + 2e' + 1/2\ O_2\ (g) \tag{1}$$

where Vö and e′ are effectively doubly and singly charged oxygen vacancy and electron, respectively. In Eq.(1) the carrier concentration[3] will increase with increasing concentration of oxygen vacancy produced by the diffusion of lattice oxygen. However, the activation energy for migration of the electron localized at donor level has been known to be 0.1–0.3 eV.[30,36,37] Therefore, it is believed that the observed activation energy (1.01 eV) in the intrinsic region consists of the total energy for migration of carrier, for diffusion of Fe ion, and for the formation of oxygen vacancy. The energy for the formation of an oxygen vacancy is small in comparison with that for the diffusion of Fe ion, since oxygen vacancies are easily produced in α-Fe_2O_3 when the diffusion of lattice Fe ions occurs.[1,3,16,34] Furthermore, according to the diffusion data reported by Salmon[1], Gardner *et al.*,[3] and Kingery *et al.*,[34] the diffusion of lattice Fe ion supports this fact, since the self-diffusion rate of Fe ion nearly equals to that of lattice oxygen. The diffusion of lattice Fe may be presented by the following

$$e' + Fe_{Fe} \rightleftharpoons Fe_i^{\cdot} \tag{2}$$

where Fe_{Fe} and $Fe_i^{\cdot}$ represent neutral Fe in lattice site and effectively singly charged Fe interstitial, respectively. If reactions(1) and (2) occur simultaneously in α-Fe_2O_3: CoO, the summation of two disorders is the form.

$$O_o + Fe_{Fe} \rightleftharpoons V_o^{\cdot\cdot} + e' + 1/2\ O_2\ (g) + Fe_i^{\cdot} \tag{3}$$

The equilibrium constant(K) in disorder(3) is

$$K = \frac{(Fe_i^{\cdot})}{(Fe_{Fe})}\,(V_o^{\cdot\cdot})\,(e')\,Po_2^{1/2} \tag{4}$$

where $(Fe_i^{\cdot})/(Fe_{Fe})$ is constant, and in disorder(1) electroneutrality condition is 2(Vö)=(e′). Substituting $C=(Fe_i^{\cdot})/(Fe_{Fe})$ and 2(Vö)=(e′) into eq.(4), and rearranging Eq.(4) for (e′), $(e')=(\frac{K}{C})^{1/2}\ Po_2^{-1/4}$. Since $\sigma \propto (e')$, the electrical conductivity dependence on Po_2 is

$$\sigma \propto Po_2^{-1/4} \tag{5}$$

$\sigma \propto Po_2^{-1/4}$ is consistent with the experimentally observed dependence in the intrinsic region at Po_2<10^{-4} atm, as shown in Table 2. Therefore, the transport mechanism is possibly explained by the disorders(1) and (2), and this mechanism can be conserved only when the two disorders(1) and (2) proceed simultaneously to reach equilibria.

Extrinsic region (Po_2>10^{-4} atm). The activation energy and $\sigma \propto Po_2^{-1/n}$ are 0.50 eV and $\sigma \propto Po_2^{-1/6}$, respectively. The ratio of the number of regular cation and anion sites in CoO and α-Fe_2O_3 is constant, respectively. Thus in CoO the ratio of regular Co and oxygen sites is 1:1 regardless of whether the actual composition is stoichiometric or nonstoichiometric. Correspondingly, in α-Fe_2O_3 the ratio of regular Fe to oxygen sites equals to 1:1.5. Through a defect reaction, 1/2 Vö is created when CoO incorporates with α-Fe_2O_3. This formation of an oxygen vacancy is presented by the reaction where $Co_{Fe}^{\cdot}$

$$Co_{Co} \rightleftharpoons Co_{Fe}^{\cdot} + \frac{1}{2}\ V_o^{\cdot\cdot} \tag{a}$$

is singly charged cobalt at Fe site. According to the principle of controlled valency, the doped Co may act as an electron acceptor, and equilibrium(a) proceeds to the right as the mol % of CoO increases. As shown in Figures (2), (4), and (7), the conductivities decrease with increasing dopping level. This indicates that another disorder may occur in this extrinsic region at Po_2>10^{-4} atm. This disorder reaction can be assumed as follows.

$$O_o \rightleftharpoons \frac{1}{2}O_2\ (g) + 2e' + V_o^{\cdot\cdot} \tag{b}$$

The increasing concentration with increasing doping in equilibrium(a) decreases oxygen vacancy concentration in equilibrium(b). The activation energy (0.50 eV) supports this fact: In the extrinsic region, Fe in regular Fe sites does not reduce, and the activation energy for the formation of oxygen vacancy is 0.4–0.3 eV, while the activation energy for the diffusion of Fe ion is estimated 0.51 eV. When the equilibrium(b) proceeds to the left due to the increasing doping level, the electron concentration in disorder (b) decreases. This decreasing electron concentration decreases the electrical conductivity, as shown in Figures (2), (4), and (7). The sum of the two disorders (a) and (b) is as follows.

$$Co_{Co} + O_o \rightleftharpoons Co_{Fe}^{\cdot} + 2e' + V_o^{\cdot\cdot} + 1/2\ O_2\ (g) + 1/2\ V_o^{\cdot\cdot} \tag{c}$$

In reaction (c), $(Co_{Fe}^{\cdot})$ and 1/2 (Vö) are determined by the doping level of CoO, and therefore, the equilibrium constant (K_c) is

$$K_C = K(V_o^{\cdot\cdot})\ n^2\ Po_2^{1/2} \tag{d}$$

where (Vö) can be replaced by 1/2 n, and rearranging Eq.(d) for n, $n = (\frac{2K_c}{K})^{1/3}\ Po_2^{-1/6}$. Since $\sigma \propto n$, the electrical conductivity dependence on Po_2 is

$$\sigma \propto Po_2^{-1/6} \tag{e}$$

$\sigma \propto Po_2^{-1/6}$ is consistent with experimentally observed

dependency in the extrinsic region at $Po_2>10^{-4}$ atm. Therefore, it is possibly suggested that the transport mechanism is the reaction (c).

Intrinsic region ($Po_2>10^{-4}$ atm). The activation energy and $\sigma \propto Po_2^{-1/n}$ are 1.01 eV and $\sigma \propto Po_2^{-1/6}$, respectively. $\sigma \propto Po_2^{-1/6}$ indicates that even at high temperatures above 400°C the reduction process (1) does not easily take place at Po_2's higher than 10^{-4} atm. $\sigma \propto Po_2^{-1/6}$ supports that the disorder reaction (2) occurs predominately, since the Po_2 dependence of electrical conductivity can be theoretically derived with the disorder reaction (2). With a view to an activation energy, however, this disorder reaction (2) requires more energy to proceed at Po_2's above 10^{-4} atm.

Acknowledgement. The authors are grateful to the Korean Science and Engineering Foundation for financial support and to Professor Ki Hyun Yoon and Dr. Hui Jun Won for helpful discussions.

References

1. O.N. Salmon, *J. Phys. Chem.* **65**, 550 (1961).
2. H. Lord and R. Parker, *Nature*, **188**, 929 (1960).
3. R.F.G. Gardner, F. Sweett, and D.W. Tanner, *J. Phys. Chem. Solids*, **24**, 1183 (1963).
4. C. Wagner and E. Koch, *Z. Phys. Chem. Abt. B*, **32(6)**, 439 (1936).
5. R.H. Chang and J.B. Wagner, Jr., *J. Am. Cer. Soc.* **55**, 211 (1972).
6. I. Bransky and A.Z. Hed, *J. Am. Cer. Soc.* **57**, 231 (1968).
7. P. Kofstad and A.Z. Hed, *J. Electrochem. Soc.* **115**, 102 (1969).
8. B.E.F. Fender and F.D. Riley, *J. Phys. Chem. Solids*, **30** 793 (1969).
9. T.A. Kovats and J.C. Walker, *Phys. Rev.* **181**, 610 (1969).
10. K.H. Kim, H.S. Han, and J.S. Choi, *J. Phys. Chem.* **83**, 1286 (1979).
11. W. Balz, Badische Anilin and Soda Fabrik., *Fr.* **1**, 357, 866 (1964).
12. K.H. Kim and J.S. Choi, *J. Phys. Chem.* **85**, 2447 (1981).
13. K.H. Kim, J.H. Jun, and J.S. Choi, *Bull. Kor. Chem. Soc.* **5**, 41 (1984).
14. K.H. Kim, D. Kim, and J.S. Choi, *J. Catalysis*, **86**, 219 (1984).
15. K.H. Kim, S.H. Lee, and J.S. Choi, *J. Phys. Chem. Solids*, **46**, 331 (1985).
16. S. Mochizuki, *Phys. State Sol. (a)* **41**, 591 (1977).
17. R.S. Sapieszko and E. Matijevic, *J. Colloid Interface Sci.* **74**, 39 (1980).
18. J.P. Reymond, P. Meriaudeau, and S.J. Teichner, *J. Catalysis*, **75**, 39 (1982).
19. J.S. Choi, K.H. Kim, and S.R. Choi, *Inter. J. Chem. Kinet.*, **9**, 489 (1977).
20. L.B. Valdes, *Proc. IRE*, **42**, 420 (1954).
21. J.S. Choi, H.Y. Lee, and K.H. Kim, *J. Phys. Chem.* **77**, 2430 (1973).
22. J.S. Choi, Y.H. Kang, and K.H. Kim, *J. Phys. Chem.* **81**, 2208 (1977).
23. K.H. Kim, S.H. Lee, Y.R. Kim, and J.S. Choi, *J. Catalysis* **88**, 283 (1984).
24. K.H. Kim, H.J. Won, and J.S. Choi, *J. Phys. Chem. Solids*, **45**, 1259 (1984).
25. K.H. Kim, E.J. Oh, and J.S. Choi, *J. Phys. Chem. Solids*, **45**, 1265 (1984).
26. K.H. Kim, K.H. Yoon, and J.S. Choi, *J. Phys. Chem. Solids*, **46**, 1061 (1985).
27. J.S. Choi, K.H. Kim, and W.Y. Chung, *J. Phys. Chem. Solids*, **47**(2), 117 (1986).
28. J.S. Choi and K.H. Yoon, *J. Phys. Chem.* **74**, 1095 (1970).
29. J.S. Choi and K.H. Kim, *J. Phys. Chem.* **88**, 666 (1976).
30. D.S. Tannhauser, *J. Phys. Chem. Solids*, **13**, 25 (1962).
31. G.H. Geiger and J.B. Wagner, Jr., Trans. AIME 233, 2092 (1965).
32. R.H. Chang and J.B. Wagner, Jr., *J. Am. Cer. Soc.* **55**, 211 (1972).
33. R.L. Coble, *J. Am. Cer. Soc.* **41**, 55 (1958).
34. W.D. Kingery, D.C. Hill, and R.P. Nelson, *J. Am. Cer. Soc.* **43**, 473 (1960).
35. S.L. Blank and J.A. Pask, *J. Am. Cer. Soc.* **52**, 669 (1969).
36. I. Bransky and D.S. Tannhauser, *Physica* **37**, 547 (1967).
37. J.H. Becker and W.R. Hosler, *Phys. Rev.* **137**, 1872 (1965).